Drug Loaded Biodegradable Load-Bearing Nanocomposites for Damaged Bone Repair

E. Y. Gutmanas[1,2,3,a)], I. Gotman[1,3,4], A. Sharipova[1,3], S. G. Psakhie[2,3], S. K. Swain[1], and R. Unger[5]

[1] Department of Materials Science and Engineering, Technion-Israel Institute of Technology, Haifa, 32000 Israel
[2] National Research Tomsk Polytechnic University, Tomsk, 634050 Russia
[3] Institute of Strength Physics and Materials Science SB RAS, Tomsk, 634055 Russia
[4] Department of Mechanical Engineering, ORT Braude College, Karmiel, Israel
[5] Institute of Pathology, University Medical Center of the Johannes Gutenberg University, Mainz, 55101 Germany

a) Corresponding author: gutmanas@technion.ac.il

Abstract. In this paper we present a short review-scientific report on processing and properties, including *in vitro* degradation, of load bearing biodegradable nanocomposites as well as of macroporous 3D scaffolds for bone ingrowth. Biodegradable implantable devices should slowly degrade over time and disappear with ingrown of natural bone replacing the synthetic graft. Compared to low strength biodegradable polymers, and brittle CaP ceramics, biodegradable CaP-polymer and CaP-metal nanocomposites, mimicking structure of natural bone, as well as strong and ductile metal nanocomposites can provide to implantable devices both strengths and toughness. Nanostructuring of biodegradable β-TCP (tricalcium phosphate)-polymer (PCL and PLA), β-TCP-metal (FeMg and FeAg) and of Fe-Ag composites was achieved employing high energy attrition milling of powder blends. Nanocomposite powders were consolidated to densities close to theoretical by high pressure consolidation at ambient temperature—cold sintering, with retention of nanoscale structure. The strength of developed nanocomposites was significantly higher as compared with microscale composites of the same or similar composition. Heat treatment at moderate temperatures in hydrogen flow resulted in retention of nanoscale structure and higher ductility. Degradation of developed biodegradable β-TCP-polymer, β-TCP-metal and of Fe-Ag nanocomposites was studied in physiological solutions. Immersion tests in Ringer's and saline solution for 4 weeks resulted in 4 to 10% weight loss and less than 50% decrease in compression or bending strength, the remaining strength being significantly higher than the values reported for other biodegradable materials. Nanostructuring of Fe-Ag based materials resulted also in an increase of degradation rate because of creation on galvanic Fe-Ag nanocouples. In cell culture experiments, the developed nanocomposites supported the attachment the human osteoblast cells and exhibited no signs of cytotoxicity. Interconnected system of nanopores formed during processing of nanocomposites was used for incorporation of drugs, including antibiotics and anticancer drugs, and can be used for loading of bioactive molecules enhancing bone ingrowth.

INTRODUCTION

The requirement for new bone to replace or restore the function of damaged or lost bone, including cases of tumor resection, is a major clinical and socioeconomic need. It is estimated that about 2 million bone-grafting procedures are performed annually worldwide [1–3]. These numbers are projected to rise steadily due to the population aging. Bone grafting is intended to stimulate bone healing and fill bone defects, with autologous bone remaining the gold standard for achieving these goals. The supply of autologous bone, however, is limited and successful healing and remodeling may not always be achieved. Furthermore, bone harvesting involves increased operative time, blood loss, postoperative pain at the donor site and length of hospital stay [4, 5]. Bone allografts eliminate donor site morbidity, however their clinical utility is limited by the risk of disease transmission and high

cost [6, 7]. The above limitations of autologous and allograft bone have initiated the search for synthetic bone graft substitutes, including scaffolds for bone ingrowth, that are placed instead of the defected bone.

Load-bearing ability of grafts is very important to avoid additional surgery, needed if implant fixation and fasteners are used and should be removed. Additional surgery is painful and requires additional expenses.

One of the research strategies in last years is development of biodegradable graft substitutes [2, 8–10]. Biodegradable implantable devices should slowly degrade over time and disappear with ingrown of natural bone replacing the synthetic graft. Finally no foreign material is left behind, allowing complete tissue regeneration without the risk of chronic inflammation or long term immune response and stress shielding related bone atrophy. Biodegradable fracture fixation devices eliminate the need of surgery for their removal.

Materials that have been considered for biodegradable implant applications include polymers such as polycaprolacton (PCL), polylactide (PLA) and polyglycolide (PGA), calcium phosphate (CaP) ceramics such as beta-TCP (tricalcium phosphate), amorphous CaP and corrodible metals such as Mg and Fe. Degradable polymers are weak, lack osteoconductivity and degrade to acidic products that can cause late inflammation [8, 9]. Biodegradable CaP ceramics are attractive materials for bone regeneration due to their close resemblance to the bone mineral, however they are intrinsically brittle and thus unsuitable for use in load-bearing sites [6, 11–13]. Moreover, introducing high porosity required for cellular ingrowth into bone regeneration scaffolds can be detrimental to the mechanical strength of the material. In the last years attempts were made to improve load-bearing capability of biodegradable CaP based ceramics by introducing a ductile and tough component (polymer or metal) into the CaP matrix, but in most cases the matrix was polymer based and the strength was still too low to use the materials in load bearing sites [14, 15].

In the last years our research team is working on development of load bearing biodegradable nanocomposites, including CaP/polymers, CaP/metals and metal/metal nanocomposites. Bone is a nanocomposite, built from matrix of ceramic HA nano-crystallites with organic collagen acting as a ductile "glue". In the case of CaP based nanocomposites nanolayers of biodegradable polymer or metal are acting as a glue, significantly improving the ductility of the composites. High strength with measurable ductility were obtained on nanocomposites with 70 vol % and more of CaP: CaP-PCL [16, 17], CaP-PLA [18, 19], CaP-FeMg [20, 21], CaP-FeAg [22] as well as on Fe-Ag [23] nanocomposites. In the case of biodegradable CaP/metal and metal/metal nanostructuring is done not only to mimic the structure of bone, that possess unique mechanical properties, but also to monitor degradation rate, especially of the metal fraction of the nanocomposite: in this case galvanic nanocouples are formed resulting in enhanced corrosion/degradation. Very high mechanical properties were achieved on Fe-Ag nanocomposites accompanied by much higher degradation rate as compared to that of pure Fe [23, 24].

In our research high energy attrition milling of powders blends is employed for nanostructuring. This is followed by cold sintering—high pressure consolidation at ambient temperature, providing retention of nanostructure and thus resulting in high mechanical properties. Both near fully dense specimens as well as macroporous 3D scaffolds were fabricated from Ca-polymer [16–19], CaP-metal [20–22] and Fe-Ag [23] nanocomposites. It was shown that methods used result in formation of interconnected system of pores that can be filled by drugs, followed by their slow release from the nanochannels.

In this paper we present a short review-scientific report on our approach for preparation of biodegradable nanocomposites for load bearing implantable devices, and results obtained on their microstructure, mechanical properties, degradation kinetics and permeability of macroporous 3D scaffolds.

EXPERIMENTAL

Details on preparation of nanostructured biodegradable Ca phosphates, tricalcium phosphate, β-TCP and Ca deficient hydroxyapatite, CDHA, can be found in [16–19]. Calcium deficient hydroxyapatite, CDHA ($Ca_9(HPO_4)(PO_4)_5(OH)$) was prepared by microwave accelerated wet method. Calcium nitrate tetrahydrate, $Ca(NO_3)_2 \cdot 4H_2O$, was dissolved in DI water at 0.5M concentration. Phosphoric acid (H_3PO_4, 85%) was added to the solution at 1.5 : 1 Ca/P ratio and stirred for 30 min. The solution was then poured into a large excess of NH_4OH to raise the pH above 10.5 and stirred for additional 30 min. The obtained precipitate was washed with DI water and heated for 15 min to complete the reaction of CDHA formation. β-TCP was obtained by thermal decomposition of the received CDHA at 750°C for 2 h:

β-TCP–PCL [16, 17], β-TCP–PLA [19] and CDHA–PLA [18] nanocomposite powders were prepared by the combination of solution-mixing and high energy attrition milling (Union Process 01HD). β-TCP-FeMg [20], β-TCP-FeAg [21] and Fe-Ag [22] nanocomposites were prepared by high energy attrition milling in hexane, at 20 : 1 balls-

to-powder ratio (2000 g of 4 mm stainless steel balls to 100 g of powder blend). Milling was conducted under Ar for 4, 8 and 12 h. Carbonyl Fe (1.0÷2.0 μm) and Ag_2O powder (<0.5 μm) were used. . Silver oxide was used instead of metallic Ag, since submicron particles of soft Ag tend to agglomerate during attrition milling which prevents their homogeneous distribution in Fe-Ag powder blend.

Schematic of processing biodegradable nanocomposites and testing of biodegradation, loading of drugs and their release is shown in Fig. 1. High energy attrition milling was followed by compaction to about 70% of theoretical density of nanocomposite blends containing metal (iron based) phase (Fig. 1a) and by high pressure consolidation/cold sintering [25, 26] of CaP-polymer nanocomposite blends (Fig. 1b). Compacts made from nanocomposite blends containing Fe based phase were annealed in hydrogen flow (usually at 450°C) to remove oxide from the surfaces of powder particles and to reduce silver oxide to pure metal. After treatment in hydrogen flow these compacts were cold sintered. Pressures of 2.5 and 3.0 GPa were used for cold sintering. Dies made from special high speed steel and from WC-15Co cemented carbides were used for high pressure consolidation. Disks 10 mm in diameter, 1.5 mm thick were prepared for bending tests and 6 mm in diameter, 5 mm thick for compression tests.

Degradation behavior of nanocomposites was studied in saline (9.00 g/l NaCl) at 37 ± 0.5°C and in Ringer's (9.00 g/l NaCl, 0.20 g/l $NaHCO_3$, 0.25 g/l $CaCl_2 \cdot H_2O$, 0.4 g/l KCl) solutions. Both solutions were prepared with double distilled water and analytically pure grade reagents. Since long immersions nanocomposites in Ringer's solution causes the deposition of a thick calcium carbonate, $CaCO_3$, layer on the specimens' surface, immersion tests were performed in saline solution, allowing accurate measurements of weight loss. 10 mm × 1.5 mm disks were placed separately into a porous net and immersed into 250 ml solution for one, two and four weeks. The solution was stirred using magnetic stirrer and its pH was maintained at 7.4 throughout the immersion experiment. After immersion, the specimens were weighed and their density and bending strength were determined. Degradation rate (mm/year) was calculated from the weight loss, according to ASTM G31-99:

$$\text{degradation rate [mm}^2\text{/year]} = \frac{8.76 \times 10^4 \times \Delta W}{A t \rho},$$

where ΔW is weight change [g], A—surface area [cm^2], t— immersion time [h], ρ—starting density [g/cm^3].

Solid corrosion products were collected by filtering the immersion solution. Ion concentration of the saline supernatant after 4 weeks immersion was measured by inductively coupled plasma optical emission spectroscopy (ICP-OES) (iCAP 6000 Series Duo ICP-OES, Thermo Scientific).

It has been demonstrated that, in the cold sintering approach, bioactive ingredients that were added to the composite blend don't lose their biological activity [27]. In [27–29] antibiotic vancomycin was incorporated in CaP-polymer nanocomposites during the stage of high energy attrition milling (see Fig. 1). In this approach processing temperature, including cold sintering and post consolidation treatments should not exceed 100°C for most antibiotics and 50°C for proteins, including antitumor doxorubicin and bone morphogenic proteins, that degrade even at slightly elevated temperatures. In present report we present also results obtained on loading/incorporation of drugs into specimens on biodegradable nanocomposites into interconnected system of nanopores under vacuum. In this case nanoporous specimens both near fully dense as well as macroporous 3D scaffolds can be prepared at higher temperatures. This may result in significantly higher mechanical properties, if during processing at elevated temperatures nanoscale structure is retained. Processing temperature of CaP-metal and Fe-Ag nanocomposites were in the range up to 800°C. Vancomycin (Vancomycin hydrochloride—VH) was used as representative of antibiotics and doxorubicin hydrochloride (DOX) was used as representative of antitumor drugs. Vancomycin hydrochloride (VH) was purchased from Acros Organics BVBA, Belgium. Doxorubicin hydrochloride (DOX) was purchased from Xi'an Leader Biochemical Engineering Co., Ltd., China. VH and DOX were dissolved in deionized water to a concentration of 10 mg/ml as stock solution. VH was added to β-TCP-PCL, β-TCP-PLA and β-TCP-FeAg nanocomposite blends, to yield 2, 5, 10 wt % of VH or DOX in the composition, and than attrition milled. The obtained blends were vacuum dried and high pressure consolidated/cold sintered at pressures up to 2.5 GPa [27–29]. In present work VH and DOX solutions of various concentration were loaded in the nanopores of 10 mm diameter cold sintered at $P = 3$ GPa disks of β-TCP-FeAg and Fe-Ag under vacuum (10^{-2} Torr).

In VH and DOX release tests drug loaded discs were immersed at 37°C 250 ml of TRIS buffer solution for one, 2 and 4 weeks. The solution was stirred using magnetic stirrer. At predetermined intervals, 5 ml aliquots were collected for examination and replaced with fresh TRIS solution. VH and DOX concentrations were evaluated using a UV spectrophotometer (Hewlett–Packard 8453) at a wavelength of 280 nm for VH and at the wavelength of 480 nm for DOX.
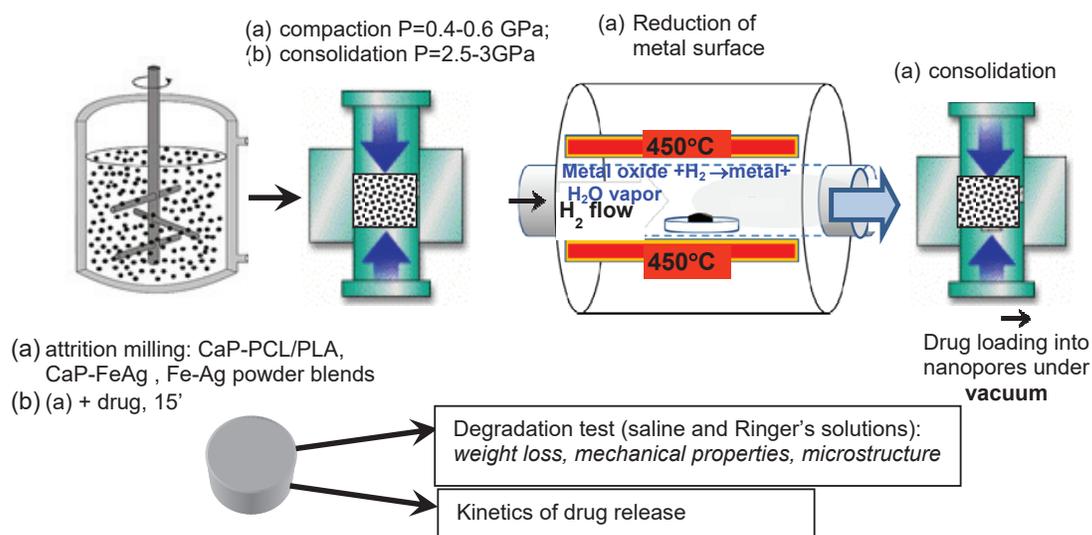
FIGURE 1. Schematic of processing and testing of biodegradable nanocomposites

VH and DOX UV calibration curves were generated using solution with VH and DOX concentration in the range of 0.5–100 μg/ml where the linear relationship between absorbance and concentration was obtained following Beer–Lambert's law. After the completion of drug release, the disks were dried and their weight and dimensions were measures to estimate degradation.

The density of consolidated specimens was determined by the Archimedes method. Mechanical properties were tested in compression and 3 point bending in an 1195 Instron testing machine. Compression tests were performed on 6 mm diameter, 3 mm high specimens at a strain rate of 10^{-5} s^{-1}; three point bending tests (8 mm span length) were performed on 10 mm diameter, 1.5 mm thick specimens at a strain rate of 2.5×10^{-5} s^{-1}. At least three specimens of each type were tested.

Phase identification of powder blends and of nanocomposites before and after immersion was done by X-ray diffraction (XRD) in an automatic powder Philips PW-1820 diffractometer with a long-focus Cu Ka tube operating at 40 kV and 40 mA. Step scans were taken over 2θ range from 25° to 75°, with a 0.02° step and a 2 s dwell time. Experimental data was compared with JCPDS standards. XRD was also used for determination of grain size of attrition milled powder blends. The experimental line broadening was corrected taking into account the internal stresses and instrumental line broadening. The microstructure of synthesized high energy attrition milled powders and of nanocomposites was characterized in a scanning electron microscope (SEM, FEI QUANTA 200) and in a high resolution SEM (HRSEM, Zeiss Ultra Plus).

In cell compatibility studies of developed biodegradable nanocomposites human osteoblast cells were seeded on 10 mm diameter discs prepared from β-TCP-FeAg and Fe-Ag nanocomposite blends. Disks were placed into 6 well plates and sterilized. Cells in 0.5 ml of medium were placed on top of each disk and incubated for 1 h at 37°C, 5% CO_2. 3 ml of medium was added to each well and the disks with cells were incubated for 48 hr. After this 10 μM Calcein AM was added into the culture medium and incubated for 10–15 min at 37°C. Calcein-AM taken up by healthy cells is converted into a strong fluorescent compound. Cells on the disks were examined by fluorescence microscopy and images were taken using a BZ-9000E fluorescent microscope.

RESULTS AND DISCUSSION

Formation of Nanocomposite Structure during Attrition Milling and Effect of Heat Treatments

High energy attrition milling results in homogeneous distribution of components, resulting in nanoscale structure. Examples of such structures obtained by high energy attrition milling followed by cold sintering at $P = 2.5$ GPa are presented in HR SEM micrographs in Fig. 2. In Fig. 2a interconnected net of PLA polymer can be clearly seen.
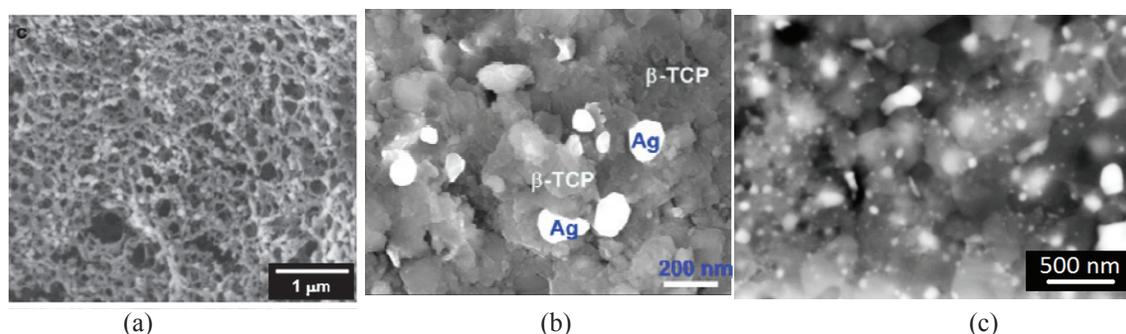
(a)   (b)   (c)

FIGURE 2. HR SEM micrographs of specimens obtained by high energy attrition milling of powder blends followed by cold sintering at P = 2.5 GPa: (a) β-TCP-20PLA (vol %), (b) β-TCP-21Fe9Ag, (c) Fe10Ag

Ductility of such net in both cases of β-TCP-PCL and β-TCP-PLA cold sintered nanocomposites results in high mechanical properties [16–18, 28]. Cold sintering of β-TCP-PLA at 120°C results in higher density/lower porosity, most of pores being open and can be filled by solution containing drugs. In Fig. 3 plots of porosity as function of PLA content of β-TCP-PLA nanocomposites cold sintered at 2.5 GPa at room temperature and 120°C are shown. It can be seen that the porosity decreases with increasing PLA content and consolidation temperature. The nanocomposites consolidated at T_{room} possess 9–11% porosity, higher values corresponding to lower PLA contents. It is plausible that at T_{room} (below T_g of PLA) the polymer doesn't flow easily even under the high pressure of 2.5 GPa and thus cannot fill the small voids between the β-TCP nanoparticles. Raising the consolidation temperature to 120°C (well above T_g of PLA) improves the polymer flow and the nanocomposite material densifies much more efficiently. A very low porosity of 3.5% was measured for the β-TCP-40PLA material consolidated at 120°C. The open porosity can be loaded by solution containing drugs under vacuum, or if drugs were added during attrition milling of the compositions nanochannels, open porosity will act as source for slow release/delivery of drugs. In Table 1 properties of consolidated β-TCP-40PLA nanocomposites without and with 1wt % vancomycin are presented. It can be seem that strength of specimens is high and especially the bending strength of specimens consolidated at 120°C.

In Fig. 2b presenting HR SEM micrograph of attrition milled β-TCP21Fe9Ag powder blend (cold sintered) uniform distribution of nanoscale metallic Fe-Ag phase and Ag nanoparticles in the β-TCP ceramic matrix is clearly seen. Uniform distribution of Fe-Ag phase and Ag nanoparticles in the β-TCP ceramic matrix was observed for other β-TCP-FeAg compositions too [22]. In [21] uniform distribution of metallic particles was observed in β-TCP-FeMg nanocomposites prepared *via* high energy attrition milling followed by cold sintering. Densities up to 98% of theoretical were obtained with nanopores forming open interconnected net. As a result of nanostructuring high strength with measurable ductility in compression and in bending were obtained. In Table 2 mechanical properties of β-TCP-FeMg and β-TCP-FeAg nanocomposites are compared with properties of β-TCP-PLA nanocomposites. Mechanical properties for β-TCP-based nanocomposites prepared by high energy attrition milling followed by cold sintering are significantly higher compared with those reported for CaP-polymer composites [13–15]. The highest bending strength was observed for β-TCP-21Fe9Ag nanocomposite. Annealing of nanocomposites at 400°C results in increase of strength and of ductility. Very uniform distribution of Ag nanoparticles in iron matrix prepared by high energy attrition milling can be seen in Fig. 2c.
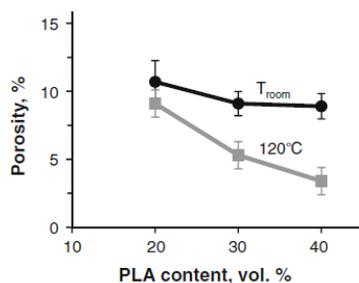

FIGURE 3. Porosity of of β-TCP-PLA nanocomposites cold sintered at 2.5 GPa as a function of PCL content and consolidation temperature

TABLE 1. Properties of β-TCP-40PLA nanocomposites without and with impregnated 1wt % vancomycin.

β-TCP-40PLA	Porosity	σ_y in compression	Bending strength
w/o VH, 2.5 GPa, T_{room}	8.9%	225 MPa	32 MPa
1 wt % VH, 2.5 GPa, T_{room}	8.9%	221 MPa	31 MPa
w/o VH, 2.5 GPa, 120°C	3.4%	229 MPa	70 MPa
1 wt % VH, 2.5 GPa, 120°C	3.4%	225 MPa	56 MPa

Densities above 95% of theoretical are obtained for Fe-5Ag and Fe-10Ag already at pressure $P = 2$ GPa (see Fig. 4). Stress-strain curves in bending for specimens of various Fe-Ag compositions cold sintered at pressure of 2.5 GPa from attrition milled blend for 8h and heat treated at 550°C for 1h and from Fe10Ag milled manually are presented in Fig. 5a. Effect of heat treatments at 600, 700 and at 800°C for 1h on stress-strain curves is presented in Fig. 5b. Such treatments result in decrease of the yield strength and increase of ductility accompanied by grain growth both of Fe and Ag.

All the compositions of Fe-Ag nanocomposites exhibited high mechanical strength in compression and in bending, the strength in compression being for Fe5Ag nanocomposites 2.35 times higher and for Fe10Ag nanocomposites 4.75 times higher than the strength of composites of the same composition but with grain size of about 25 μm [30].

Taking into account that the strength of developed bioresorbbale CaP-polymer, CaP-metal and metal-metal nanocomposites is close or even higher than the strength of human cortical bone [31, 32], the developed materials can be used for fabrication of load bearing orthopedic implants.

Degradation Behavior of Developed Biodegradable Nanocomposites

Degradation behavior of β-TCP-PLA with different PLA contents as fabricated (dry) and after one week immersion in TRIS buffer solution at 37°C (wet) is shown in Fig. 6 [18]. An approximately 40% decrease of compressive strength is evident after one week immersion. No additional decrease of compressive strength was observed when the specimens were immersed in TRIS for 4 weeks. As can be seen in Fig. 5 the decrease in strength is accompanied by an increase in ductility being especially pronounced in the 20 and 30 vol % PLA nanocomposites. After 4 weeks of immersion/degradation test the retained strength is significantly higher than that obtained on biodegradable CaP-PLA composites in other research reports [31, 32]. Immersion in Ringer's solution of β-TCP-FeMg nanocomposites resulted in gradual decrease of bending strength with immersion time (Fig. 7) [20]. The moderate loss in strength of 12.5–15% measured after 7 days immersion in Ringer's solution is significantly less than the >50% drop of strength exhibited by the polymer-reinforced β-TCP-30PLA (in compression [18]) and HA-30PLA (in bending [15]) composites after the same immersion period.
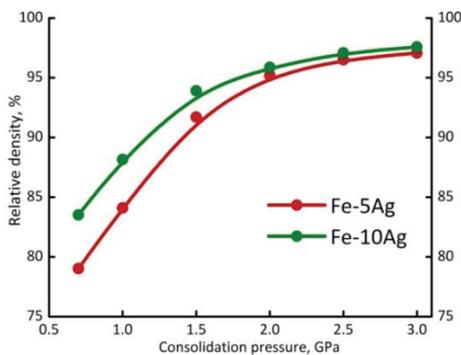

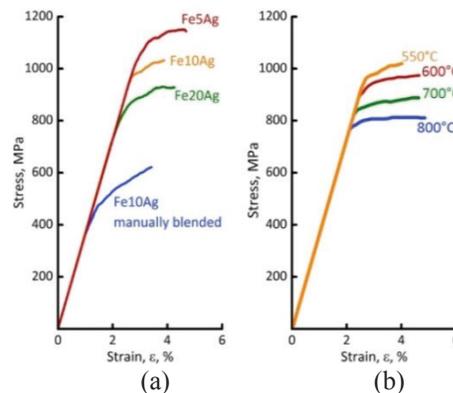**FIGURE 4.** Density of Fe-5Ag and Fe-10Ag as a function of consolidation pressure

FIGURE 5. Bending strength of Fe-Ag (a) for various compositions, (b) for Fe-10Ag as a function of heat treatments for 1 h at 550, 600, 700 and at 800°C

TABLE 2. Mechanical properties of the synthesized β-TCP-metal nanocomposites

Composition and processing	Compressive strength, MPa	Plastic strain in compression, %	Bending strength, MPa	Relative density, % TD
βTCP-15Fe15Mg, as-cold sintered (c.s.)	420 ± 17	2.9	163 ± 10	96 ± 0.5
βTCP-24Fe6Mg, c.s.	270 ± 12	5.8	120 ± 6	95 ± 0.6
βTCP-15Fe15Mg, c.s. + 400°C, 4 h	470 ± 20	3.6	165 ± 13	98 ± 0.5
βTCP-24Fe6Mg, c.s. + 400°C, 4 h	350 ± 15	6.7	140 ± 8	97 ± 0.4
βTCP-30Mg, c.s.	540 ± 20	0.5	132 ± 15	94 ± 0.5
βTCP-30Mg, c.s. + 400°C, 4 h	520 ± 23	0.2	110 ± 18	95 ± 0.6
β-TCP-21Fe9Ag, c.s. + 400°C, 4 h	570 ± 20	3.2	222 ± 15	98 ± 0.5
β-TCP-24Fe6Ag, c.s. + 400°C, 4 h	499 ± 16	2.4	171 ± 8	97 ± 0.3
β-TCP-27Fe3Ag, c.s. + 400°C, 4 h	460 ± 22	1.9	158 ± 13	96 ± 0.6
β-TCP-30Fe, c.s. + 400°C, 4 h	360 ± 15	1.1	135 ± 5	95 ± 0.5
β-TCP-30PLA [18]	330	2.0	62	96

After 4 weeks days immersion, the β-TCP-15Fe15Mg and β-TCP-24Fe6Mg specimens lost, respectively, 53 and 60% of their initial strength. Such strength reduction must be due to the increase in porosity (decrease in relative density), especially prominent for the β-TCP-24Fe6Mg composition. The degradation behavior of both β-TCP-FeMg compositions is in sharp contrast to that of the β-TCP-based composite reinforced with pure Mg, β-TCP-30Mg. These latter specimens lost strength catastrophically and disintegrated completely as early as after 2 days immersion in Ringer's solution. Such catastrophic degradation must be due to hydrogen evolution during the rapid corrosion of the large amount (30 vol %) of the uniformly distributed, interconnected submicron Mg particles.

For all the specimens of β-TCP-FeAg nanocomposites, the direct weight loss after 4 weeks (28 days) immersion was comparable with the weight of Fe metal needed to form the Fe_3O_4 sediment extracted from the solution. All the Ag-containing specimens exhibited greater weight loss compared to the Ag-free β-TCP-30Fe material, presumably due to the galvanic action of silver dispersed in the iron phase. Among the Ag-containing specimens, those with the smallest Ag content (β-TCP-27Fe3Ag, 10% Ag in the metal phase) exhibited the highest degradation rate - four fold that of the β-TCP-30Fe composition. Three-point bending strength, σ_b, of β-TCP-30Fe and β-TCP-30(Fe-Ag) nanocomposites after different immersion times is shown in Fig. 8. For all the compositions, the bending strength decreases with immersion time reaching approximately 50% of the initial value after 28 days. Still, the β-TCP-FeAg nanocomposites remain significantly stronger, both in compression and bending, than the corresponding β-TCP-24Fe6Mg [20] and β-TCP-30PLA [18] materials after the same immersion period.

Biodegradable metals such as Mg and Fe are strong and ductile as compared to biodegradable polymers and ceramics. Fe based alloys possess superior strength compared to Mg based alloys, and their microstructure and properties can be tailored using controlled heat treatments. Fe-based materials have been investigated as candidates for biodegradable cardiovascular stents [33, 34] and orthopedic implants including macroporous scaffolds [35, 36].
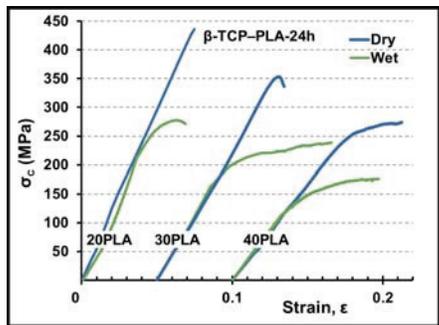

FIGURE 6. Degradation behavior of β-TCP-PLA with different PLA contents: as fabricated (dry) and after one week immersion in TRIS buffer solution at 37°C (wet) [18]
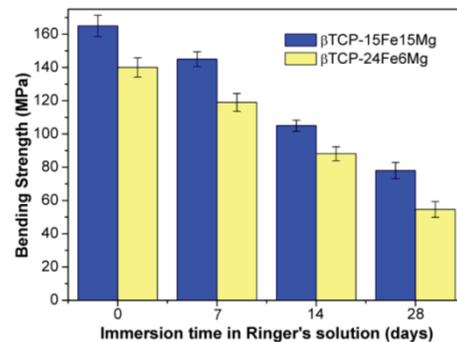

FIGURE 7. Degradation behavior (bending strength) of β-TCP-FeMg nanocomposites after different immersion exposures in Ringer's solution
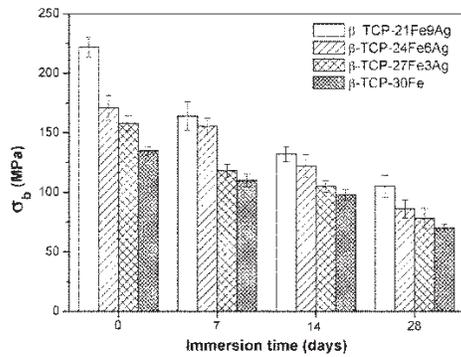
FIGURE 8. Degradation behavior (bending strength) of β-TCP-FeAg nanocomposites after different immersion exposures in saline solution [21]
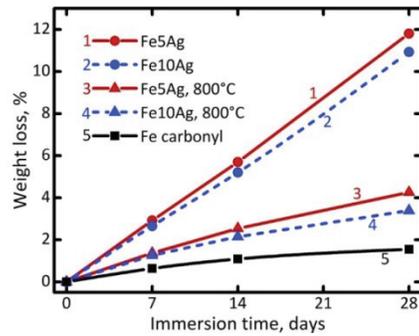

FIGURE 9. Weight loss as a function of immersion time of FeAg nanocomposites: (*1*) Fe5Ag and (*2*) Fe10Ag heat treated 550°C, 1 h; (*3*) Fe5Ag and (*4*) Fe10Ag heat treated at 800°C, 1 h; (*5*) carbonyl iron

The main challenge to overcome is the too low corrosion rate of iron in biological environment [30, 36, 37]. In the case of biodegradable Fe-Ag nanocomposites, silver nanoparticles may act as an antimicrobial agent as well as act as cathodic sites towards iron formic galvanic nanacouples. Weight loss obtained by directly weighing the specimens after different immersion periods in saline solution is presented in Fig. 9. For both nanocomposites, Fe5Ag and Fe10Ag heat treated at 550°C (curves *1* and *2* in Fig. 9), direct weight loss was more than 2 times higher than that in dissolution test of β-TCP-FeAg nanocomposites [21]. Weight loss for Fe5Ag and Fe10Ag heat treated at 800°C (curves *3* and *4* in Fig. 9) and weight loss of 1.0÷2.0 μm carbonyl iron (curve *5*) was significantly lower as compared to Fe5Ag and Fe10Ag nanocomposites, indicating importance of nanostructuring and presence of galvanic Fe-Ag nanocouples to achieve high corrosion rate of iron. Degradation rate calculated from direct weight loss after 28 day for Fe-Ag nanocomposites heat treated at 550°C was 2.22 mg/cm2 per day for Fe5Ag specimens and 2.09 mg/cm2 per day for Fe10Ag specimens. These numbers of degradation rate are 9 times higher than reported results on degradation rate of Fe5Ag and Fe10Ag composites with grain size of about 25 μm after 30 days immersion in Hank's solution [30].

Loading and Release of Vancomycin and Doxorubicin from Nanopores of Biodegradable Nanocomposites

In Fig. 10, cumulative vancomycin release in TRIS solution from β-TCP-40PLA-VH nanocomposites cold sintered at T_{room} and at 120°C is presented (VH was introduced during attrition milling of the powder blend). Gradual release was observed for both materials, with 94 and 83% total vancomycin load released in 5 weeks from the specimens consolidated at T_{room} and 120°C, respectively. Over the same time period, the mass loss of the specimens did not exceed 2% (including 1 wt % VH) suggesting that the release of vancomycin from β-TCP-40PLA nanocomposites is realized by diffusion rather than by material degradation.
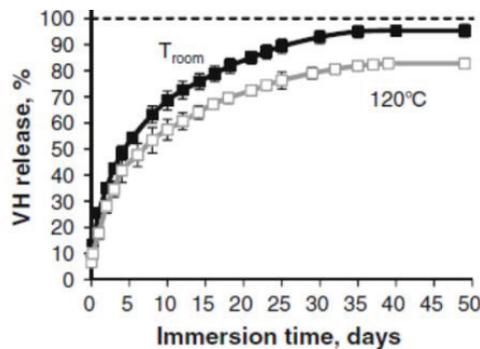

FIGURE10. Cumulative vancomycin release from β -TCP-40PLA-VH nanocomposites as a function of immersion time in TRIS buffer solution at 37°C
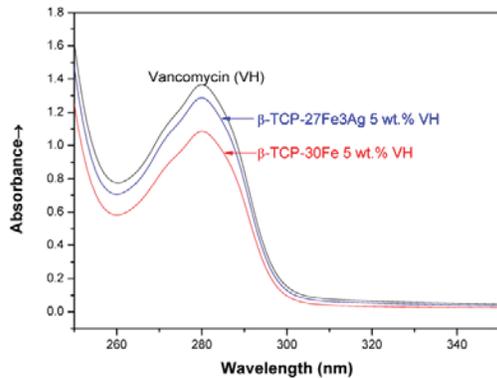
FIGURE 11. UV spectrophotometer calibration curves for vancomycin (VH), β-TCP-27Fe3Ag-5%VH and β-TCP-30Fe-5%VH
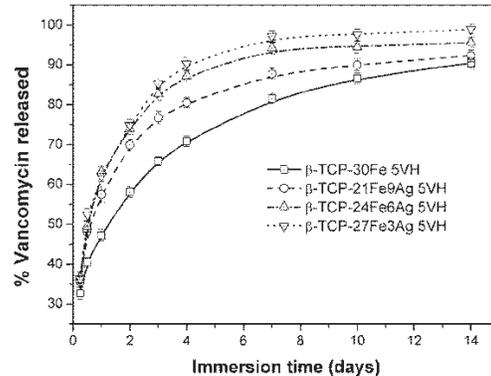

FIGURE 12. Cumulative release from disks of nanocomposites β-TCP-(FeAg) containing 5 wt % VH as a function of immersion time in TRIS buffer solution at 37°C

The results of the antimicrobial tests show that vancomycin released from our cold sintered β-TCP-40PLA nanocomposites is effective in killing *S. aureus* bacteria [29].UV spectrophotometer calibration curves for vancomycin (VH), β-TCP-27Fe3Ag-5%VH and β-TCP-30Fe-5%VH are shown in Fig. 11. Vancomycin (VH) was loaded into nanoposes under vacuum. VH release profile as function of time is shown in Fig. 12 Vancomycin released ~35% of the total drug loaded in the initial burst, and remaining 65% in the period of 6–8 days in β-TCP-30(Fe-Ag) nanocomposite specimens. β-TCP-30Fe specimens eluted ~30% within the initial burst and the gradual released with 90% VH over the period of 2 weeks. For Ag-containing specimens, those with the lowest Ag content (β-TCP-27Fe3Ag) show faster release of VH probably because of higher porosity and faster degradation rate due to the nanogalvanic couples Fe-Ag formed by silver nanoparticles dispersed in the iron matrix (Fig. 2b) [22]. An attractive gradual release of VH is observed with >90% release after 2 weeks immersion for all compositions containing Ag.

UV spectrophotometer calibration curves for doxorubicin (DOX), β-TCP, β-TCP-PLA, β-TCP-27Fe3Ag and β-TCP-30Fe, are shown in Fig. 13. (DOX was loaded into nanopores under vacuum). It can be seen that for nanocomposites containing iron UV signal corresponding to DOX (at 480 nm) is very low. Doxorubicin forms complexes with iron [38, 39], that are not detected in UV-visible light range. Doxorubicin release profile as function of time is shown in Fig. 14. It can be seen that gradual release of large part of loaded DOX from β-TCP and β-TCP-PLA takes place during 2 weeks. Release of DOX from nanocomposite containing iron, β-TCP-27Fe3Ag, is very low, indicating that UV spectroscopy is not detecting the DOX-iron complexes, or that most of DOX molecules are tight to iron forming complexes inside of nanochannels of the nanocomposite. According to literature doxorubicin-metal complexes retain their efficacy as anticancer drug [40]. Still in case when most of DOX molecules are tight to iron in nanochannels, their release can take place only with degradation of the biodegradable implantable device, and to provide required rate of DOX supply the rate of degradation of the biodegradable nanocomposite should be high enough. Formation and stability of the DOX—metal nanocomplexes can be studied *in silico* using molecular dynamics simulations, as it is conducted for soft matter—hard matter complexes [41].
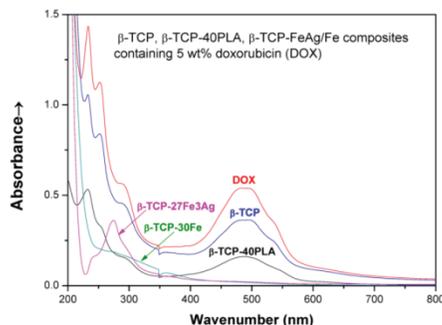

FIGURE 13. UV spectrophotometer calibration curves for doxorubicin (DOX), β-TCP, β-TCP-PLA, β-TCP-27Fe3Ag and β-TCP-30Fe,
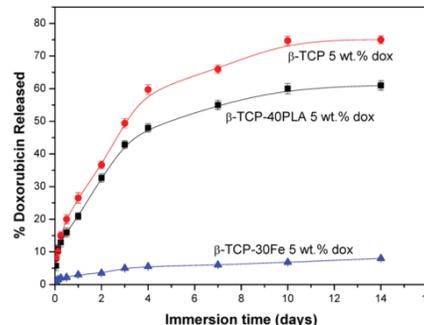

FIGURE 14. Cumulative DOX release from disks of β-TCP, β-TCP-40PLA and β-TCP-30Fe, containing 5 wt % DOX as a function of immersion time in TRIS buffer solution at 37°C
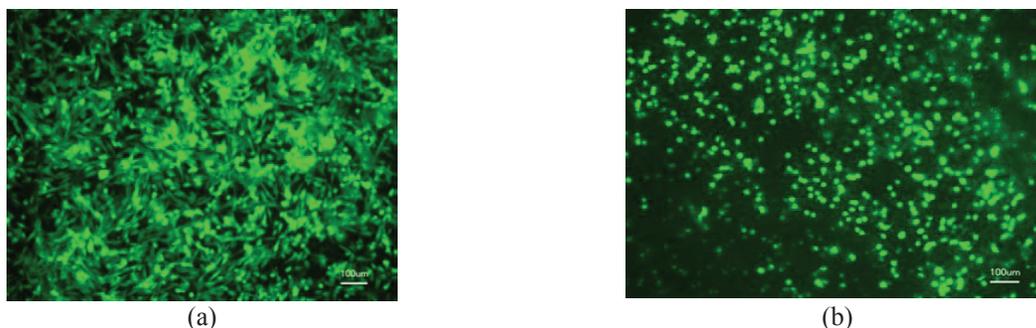
FIGURE 15. Fluorescent images of human osteoblasts growing on (a) ß-TCP-27Fe3Ag and (b) Fe10Ag nanocomposite disks. Cells were added to the disks placed in plastic petri plates and at particular time points the cells on the disks were stained with Calcein-AM. Images show cells on the disks at 48 h

Cell Culture Experiments

Examples of microscopic evaluation and images after Calcein-AM staining showed that human osteoblast cells stayed adhered to the disks of β-TCP-27Fe3Ag and Fe10Ag nanocomposite after 48 h (Fig. 15). After longer exposures decrease in attached cells was observed on the disks. The decrease was not due to cytotoxic components leaching from the materials—this was verified by the absence of cell death growing next to the discs. All cells exhibited a normal cell-staining pattern after addition of calcein-AM and resembled control cells on well plastic, that had not been exposed to the β-TCP-27Fe3Ag and Fe10Ag nanocomposites. The obtained results indicate that the developed β-TCP-27Fe3Ag and Fe10Ag nanocomposites show no signs of cytotoxicity and can be used as implant materials.

CONCLUSIONS

Load bearing biodegradable β-TCP-polymer, β-TCP-FeMg/FeAg and Fe-Ag were developed employing high energy attrition milling followed by high pressure consolidation at ambient temperature—cold sintering. Strength of developed nanocomposites is in the range of human bone and is considerably higher than reported results obtained on other biodegradable materials. Degradation rates in desirable range where obtained for developed biodegradable nanocomposites—thus mechanical support for successful bone repair can be provided over time of synthetic graft degradation. Developed load bearing biodegradable nanocomposites can be used for controlled antibiotic and anticancer drug release by incorporation of drugs into nanochannells of implantable devices.

REFERENCES

1. C. T. Laurencin, Y. Khan, and S. F. El-Amin, Expert Rev. Med. Devices **3**(1), 49–57 (2006).
2. M. Bohner, Mater. Today **13**(1-2), 24–30 (2010).
3. R. A. Bhatt and T. D. Rozental, Hand Clin. **28**, 457–468 (2012).
4. D. I. Ilan and A. l. Ladd, Oper. Tech. Plast. Reconstr. Surg. **9**, 151–160 (2003).
5. T. A. StJohn, A. R. Vaccaro, A. P. Sah, M. Schaefer, S. C. Berta, et el., Am. J. Orthop. **32**, 18–23 (2003).
6. P. Ducheyne and Q. Quo, Biomaterials **20**, 2287–2303 (1999).
7. K. D. Johnson, K. F. Frierson, T. S. Keller, C. Cook, R. Scheinberg, et al., J. Orthop. Res. **14**, 351–369 (1996).
8. A. Gloria, R. De Santis, and L. Ambrosio, J. Appl. Biomater. Biomech. **8**(2), 57–67 (2010).
9. J. Iqbal, Y. Onuma, J. Ormiston, A. Abizaid, R. Waksman, and P. Serruys, Eur. Heart J. **35**, 765–776 (2014).
10. F. Witte, Acta Biomater. **6**, 1680–1692 (2010).
11. J. H. Shepherd and S. M. Best, JOM **63**(4), 83–92 (2011).
12. W. G. De Long, T. A. Einhorn, K. Koval, M. McKee, W. Smith, R. Sanders, and T. Watson, J. Bone Joint Surg. **89**, 649–658 (2007).
13. A. J. Wagoner Johnson and B. A. Herschler, Acta Biomater. **7**, 16–30 (2011).
14. Y. Shikinami and M. Okuno, Biomaterials **20**, 859–877 (1999).
15. J. Russias, E. Saiz, R. Nalla, K. Gryn, R. Ritchie, and A. P. Tomsia, Mater. Sci. Eng. C **26**, 1289–1295 (2006).

16. C. Makarov, I. Gotman, X. Jiang, S. Fuchs, C. J. Kirkpatrick, and E. Y. Gutmanas, J. Mater. Sci. Mater. Med. **21**, 1771–1779 (2010).
17. M. Bernstein, I. Gotman, C. Makarov, A. Phadke, S. Radin, P. Ducheyne, and E. Y. Gutmanas, Adv. Eng. Mater. **12**, B341–347 (2010).
18. A. Rakovsky, I. Gotman, E. Rabkin, and E. Y. Gutmanas, J. Mech. Behav. Biomed. Mater. **18**, 37–46 (2013).
19. A. Rakovsky, I. Gotman, E. Rabkin, and E. Y. Gutmanas, J. Mech. Behav. Biomed. Mater. **32**, 89–98 (2014).
20. S. K. Swain, I. Gotman, and E. Y. Gutmanas, Adv. Biomater. Devices Med. **2**, 55–62 (2015).
21. S. K. Swain, I. Gotman, R. Unger, C. J. Kirkpatrick, and E. Y. Gutmanas, J. Mech. Behav. Biomed. Mater. **53**, 434–444 (2016).
22. S. K. Swain, I. Gotman, R. Unger, and E. Y. Gutmanas, Mater. Sci. Eng. C **78**, 88–95 (2017).
23. A. Sharipova, S. G. Psakhie, S. K. Swain, I. Gotman, and E. Y. Gutmanas, AIP Conf. Proc. **1683**, Article Number UNSP 020244 (American Institute of Physics, Melville, NY, 2015).
24. I. Gotman, S. K. Swain, A. Sharipova, and E. Y. Gutmanas, AIP Conf. Proc. **1783**, 020062 (2016). doi 10.1063/1.4966355
25. E. Y. Gutmanas, A. Rabinkin, and M. Roitberg, Scripta Metall. **13**, 11–15 (1979).
26. E. Y. Gutmanas, Powder Met. Int. **15**, 129–132 (1983).
27. C. Makarov, V. Cohen, A. Raz-Pasteur, and I. Gotman, Eur. J. Pharm. Sci. **62**, 49–56 (2014).
28. C. Makarov, I. Gotman, S. Radin, P. Ducheyne, and E. Y. Gutmanas, J. Mater. Sci. **45**, 6320–6324 (2010).
29. C. Makarov, I. Berdicevsky, A. Raz-Pasteur and I. Gotman, J. Mater. Sci.: Mater. Med. **24**, 679-87 (2013).
30. T. Huang, J. Cheng, D. Bian, and Y. Zheng, J. Biomed. Mater. Res. **104B**, 225–240 (2016).
31. R. E. Neuendorf, E. Saiz, A. P. Tomsia, and R. O. Ritchie, Acta Biomater. **4**, 1288–1296 (2008).
32. S. I. J. Wilberforce, C. E. Finlayson, S. M. Best, and R. E. Cameron, J. Mech. Behav. Biomed. Mater. **4**, 1081–1089 (2011).
33. M. Peuster, C. Hesse, T. Schloo, C. Fink, P. Beerbaum, and C. V. Schnakenburg, Biomater. **27**, 4955–-4962 (2006).
34. R. Waksman, R. Pakala, R. Baffour, R. Seabron, D. Hellnga, and F. O. Tio, J. Interv. Card. **21**, 15–20 (2008).
35. T. Kraus, F. Moszner, S. Fischerauer, M. Fiedler, E. Martinelli, J. Eichler, F. Witte, E. Willbold, M. Schinhammer, M. Meischel, P. J. Uggowitzer, J. F. Löffler, and A. Weinberg, Acta Biomater. **10**, 3346–3353 (2014).
36. B. Wegener, B. Sievers, S. Utzschneider, P. Müller, V. Jansson, S. Rößler, B. Nies, G. Stephani, B. Kieback, and P. Quadbeck, Mater. Sci. Eng. B **176**, 1789–1796 (2011).
37. M. Schinhammer, A. C. Hanzi, J. F. Loffler, and P. J. Uggowitzer, Acta Biomater. **6**, 1705–1713 (2010).
38. C. E. Myers, L. Gianni, C. B. Simone, R. Klecker, and R. Greene, Biochemistry **21**, 1707–1713 (1982).
39. D. R. Richardson, P. C. Sharpe, D. B. Lovejoy, D. Senaratne, D. S. Kalinowski, M. Islam, and P. V. Bernhardt, J. Med. Chem. **49**, 6510–6521 (2006).
40. E. Munnier, S. Cohen-Jonathan, K. Herve, C. Linassier, M. Souce, P. Dubois, and I. Chourpa, J. Nanopart. Res. **13**, 959–971 (2011).
41. A. A. Tsukanov and S. G. Psakhie, Phys. Mesomech. **20**(1), 43–54 (2017).